AD

TECHNICAL REPORT ARCCB-TR-97007

FATIGUE ANALYSIS OF A VESSEL EXPERIENCING PRESSURE OSCILLATIONS

EDWARD TROIANO
JOHN H. UNDERWOOD
ANTHONY SCALISE
G. PETER O'HARA
DANIEL CRAYON

MARCH 1997

US ARMY ARMAMENT RESEARCH,
DEVELOPMENT AND ENGINEERING CENTER
CLOSE COMBAT ARMAMENTS CENTER
BENÉT LABORATORIES
WATERVLIET, N.Y. 12189-4050

APPROVED FOR PUBLIC RELEASE; DISTRIBUTION UNLIMITED

DISCLAIMER

The findings in this report are not to be construed as an official Department of the Army position unless so designated by other authorized documents.

The use of trade name(s) and/or manufacturer(s) does not constitute an official indorsement or approval.

DESTRUCTION NOTICE

For classified documents, follow the procedures in DoD 5200.22-M, Industrial Security Manual, Section II-19 or DoD 5200.1-R, Information Security Program Regulation, Chapter IX.

For unclassified, limited documents, destroy by any method that will prevent disclosure of contents or reconstruction of the document.

For unclassified, unlimited documents, destroy when the report is no longer needed. Do not return it to the originator.

REPORT DOCUMENTATION PAGE

Form Approved
OMB No. 0704-0188

1. AGENCY USE ONLY (Leave blank)	2. REPORT DATE	3. REPORT TYPE AND DATES COVERED
	March 1997	Final

4. TITLE AND SUBTITLE
FATIGUE ANALYSIS OF A VESSEL
EXPERIENCING PRESSURE OSCILLATIONS

5. FUNDING NUMBERS
AMCMS No. 6226.24.H180.000
PRON No. TU5B5F261ABJ

6. AUTHOR(S)

Edward Troiano, John H. Underwood, Anthony Scalise,
G. Peter O'Hara, and Daniel Crayon

7. PERFORMING ORGANIZATION NAME(S) AND ADDRESS(ES)

U.S. Army ARDEC
Benet Laboratories, AMSTA-AR-CCB-O
Watervliet, NY 12189-4050

8. PERFORMING ORGANIZATION REPORT NUMBER

ARCCB-TR-97007

9. SPONSORING / MONITORING AGENCY NAME(S) AND ADDRESS(ES)

U.S. Army ARDEC
Close Combat Armaments Center
Picatinny Arsenal, NJ 07806-5000

10. SPONSORING / MONITORING AGENCY REPORT NUMBER

11. SUPPLEMENTARY NOTES

Presented at the ASTM 28th National Symposium on Fatigue and Fracture Mechanics. Saratoga, NY, 25-27 June 1996.
Published in *ASTM STP 1321, Fatigue and Fracture Mechanics, 28th Volume*.

12a. DISTRIBUTION / AVAILABILITY STATEMENT

Approved for public release; distribution unlimited.

12b. DISTRIBUTION CODE

13. ABSTRACT *(Maximum 200 words)*

A pressure vessel, which was designed and tested under laboratory conditions for tens of thousands of cycles, failed in service after only a few cycles. Thousands of oscillatory pressure reversals were measured at each loading. However, the predominance of the stress amplitudes were well below the critical threshold values necessary to initiate fatigue cracking.

Analysis demonstrated that the disparity between lab cycling and field loading conditions could not be explained simply by mechanical loading alone. Further investigation into the problem revealed that an extremely aggressive environment, the by-products of the internal combustion from within the pressure vessel, along with high temperatures, pressures, and other sources of high tensile loading all contributed to the short fatigue life of the vessel.

14. SUBJECT TERMS
Low-Cycle Fatigue, Pressure Oscillations, Pressure Vessels, Cumulative Damage Model, Residual Stresses, Hoop Stress, Radial Stress, Fatigue Cracks, Palmgren-Miner Rule, Environmentally-Assisted Cracking

15. NUMBER OF PAGES
16

16. PRICE CODE

17. SECURITY CLASSIFICATION OF REPORT	18. SECURITY CLASSIFICATION OF THIS PAGE	19. SECURITY CLASSIFICATION OF ABSTRACT	20. LIMITATION OF ABSTRACT
UNCLASSIFIED	UNCLASSIFIED	UNCLASSIFIED	UL

TABLE OF CONTENTS

TABLES

LIST OF ILLUSTRATIONS

INTRODUCTION

It is often necessary to connect sections of a pressure vessel in order to attain the required configuration of the overall component. This connection requires some form of sealing at the section interfaces to preserve continuity and to produce a leakproof joint (Figure 1). The oil and piping industries have sought various types of connectors that provide such a leakproof joint. [1,2]

Sealing of pressure vessel sections in cannons is further complicated by the presence of pressure oscillations associated with the combustion process. As many as two thousand pressure reversals have been observed during each firing cycle. This report addresses several important issues related to sealing of pressure vessels experiencing such oscillations, including:

- The effect of the pressure oscillations on the overall life of the pressure vessel
- The source of the tensile loads that cause failure
- The role of environmentally-assisted cracking and its impact on failures
- Conclusions and recommendations necessary to prevent further failures

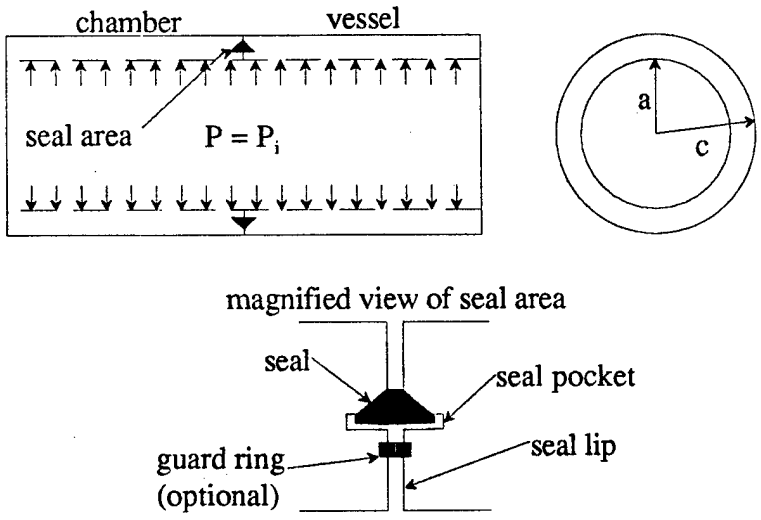

Figure 1. Schematic of seal concept, geometry, and loading.

HISTORICAL PERSPECTIVE

Historically, large caliber thick-walled cannon pressure vessels, such as the type investigated here, have required only a simple mechanical wedge block assembly to completely seal the rear face of the pressure vessel. For various reasons, the use of a wedge block was deemed impractical for this application—forcing the designers to pursue other means of sealing. The sections to be sealed are hereafter referred to as the chamber

and the vessel (Figure 1). The chamber material is PH 13-8Mo stainless steel heat treated to 1276 MPa, and the vessel is A723 Grade 2 steel heat treated to 1172 MPa. Other mechanical properties are shown in Table 1. The seal is 17-4 PH stainless steel heat treated to 627 MPa. The vessel has been mechanically autofrettaged so that the elastic/plastic boundary is 55 percent through the vessel wall. Basic geometric features include an internal radius of 78 mm and an outside radius of 162 mm. Internal peak pressures are nominally 405 MPa.

Table 1. Properties of Materials Investigated

Material	Tensile Strength, σ_{UTS} (MPa)	0.2%Yield Strength, σ_{YS} (MPa)	Young's Modulus, E (GPa)	Strain @ 10^6 Cycles [3] (%)	True Fracture Strain [4] (%)
PH 13-8Mo	1344	1276	200	0.241	15.0
A723	1275	1172	207	0.167	14.6

The detailed sealing concepts investigated in this study are described in Figure 2. The original sealing concept (configuration #1) included a two-surface wedge seal encased in a rectangular shaped seal pocket at the radial wall location, r/c, of 0.68. Configuration #1 also included a guard ring located at the radial wall location of 0.62. The guard ring possessed four through holes located at 0°, 90°, 180°, and 270° from the top center

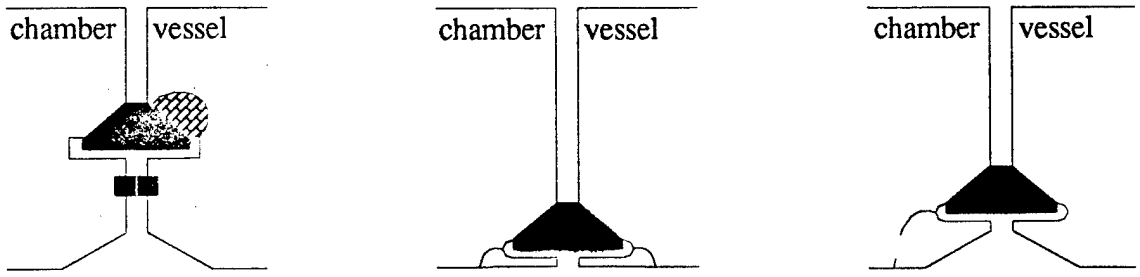

configuration #1
C-R crack orientation
5 cycles

configuration #2
R-L crack orientation
30 cycles

configuration #3
R-L crack orientation
100 cycles

Figure 2. Historical perspective of seal configurations.

position of the pressure vessel. The guard ring provides a barrier between the internal combustion by-products and the seal. The through holes in the guard ring allow pressure to enter the seal pocket and force the two seal surfaces against their mating surfaces on the chamber and vessel, respectively. Cracking in the vessel portion of configuration #1 was observed after only five loading cycles. Cracking initiated at a mid-wall location

emanating from the rectangular seal pocket in the C-R orientation (a plane perpendicular to the circumferential direction, with crack growth predominately in the radial direction). At the time of the failure very little was known about the nature of the pressure oscillations. The cracking was in an area of known tensile stresses, including applied hoop firing stresses and residual hoop autofrettage stresses. Although the combination of applied and residual stresses was well below the yield strength of the vessel material (see stress versus wall location plot in Figure 3), the sharp stress riser of the rectangular seal pocket may have concentrated the local stresses to about the level of the yield stress. At this time further investigation of configuration #1 was halted because the source of the stresses and the failure had been characterized well enough to proceed to configuration #2.

The configuration #2 concept used the lessons learned in configuration #1 to make significant improvements to the seal area. Major changes included moving the seal closer to the inside diameter of the vessel and chamber to a radial wall location of 0.55 and removing the rectangular seal pocket in lieu of a semicircular (r = 3.2 mm) seal pocket. As seen in the plot of Figure 3, the configuration #2 seal and seal pocket are at a location of nearly zero hoop stresses. The semicircular seal pocket reduced the local high stresses that resulted from the sharp stress concentrator, which may have contributed to the failure of configuration #1. Seal lips integral to both the chamber and vessel replaced the guard ring to protect the seal. Configuration #2 cracked after approximately 30 loading cycles.

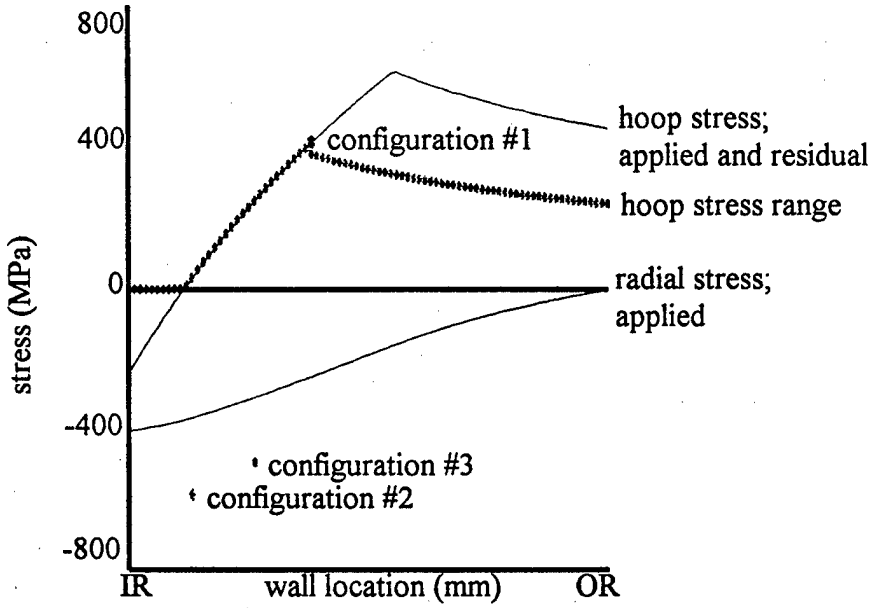

Figure 3. Theoretical stress distribution taking into effect Lamé stresses and autofrettage stresses; points indicate effects of K_t.

Cracking initiated in the chamber and vessel at the root of the seal pocket notch, in the R-L orientation (a plane perpendicular to the radial direction, with crack growth predominately in the longitudinal direction). Both seal pockets had nearly identical cracks at the same radial location; these cracks eventually grew approximately 50 mm in length along the root of the seal pockets. During testing of configuration #2, the presence of pressure oscillations became evident. However, as with configuration #1, the full extent of the pressure oscillations was not understood.

Configuration #3 had the same seal and seal pocket as configuration #2. The main difference was that the location of the seal was now at a radial wall location of 0.62. Although clearly not in as favorable a hoop stress region, this wall location allowed designers the opportunity to provide a stiffer seal lip and the necessary protection for the seal itself. After 100 loading cycles, configuration #3 failed in a similar fashion to configuration #2. A radial stress-induced crack (R-L orientation) emanated from the root of the seal pocket on the chamber side and grew approximately 50 mm in length until a section of the seal lip became dislodged. Unlike the failure of configuration #1, the source of the radial stress that initiated the crack was not known, and proprietary concerns prevented any definitive investigation. An analysis of possible sources of radial stresses near the seal is given below. During testing of configuration #3, the full extent of the pressure oscillations became evident. The extent of these pressure oscillations will also be discussed below.

OSCILLATION BEHAVIOR

Typically, large caliber cannon pressure vessels, such as the one investigated here, experience a pressure versus time trace that is relatively smooth and of a sinusoidal waveform— rising from zero to peak pressure and back to zero in approximately 0.05 second. Oscillations are often observed during a normal loading cycle. However, the relative number and magnitude of these oscillations are typically very small. The vessel and chamber investigated here experienced a different, more complex loading history. A strain range-time plot (as measured by hoop strain gages placed on the outside diameter of the chamber) is shown in Figure 4. In this case, more than 1400 strain reversals were measured; however, in other cases as many as 2000 strain reversals have been recorded. One of the major concerns with this loading history is that the magnitudes of some of the strain reversals have exceeded the average nominal strain that is typically experienced. The data for configuration #1, depicted in Figure 4, were analyzed, and a histogram of the number of occurrences at each strain range and R-ratio was made. (These nominal strains were also used to calculate local strains for configurations #2 and #3.) The results are shown in Figure 5. Analysis of the histogram shows that 68 percent of occurrences are within the 0 to 5 percent of maximum strain range, and 90 percent of the occurrences occur between 0 and 15 percent of the maximum strain range.

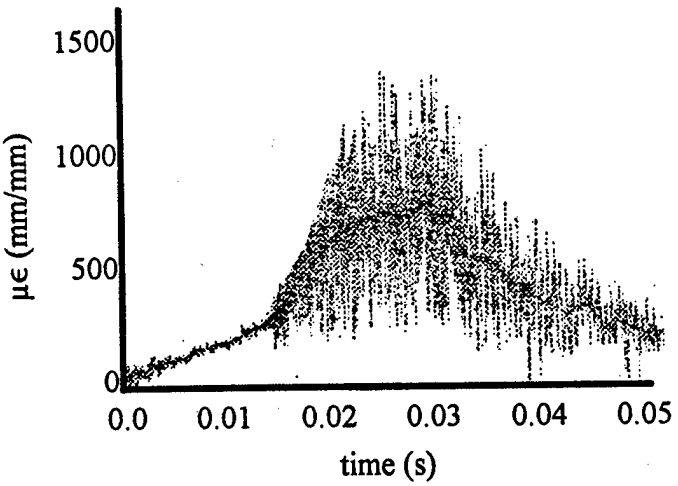

Figure 4. Typical strain versus time plot showing loading oscillations.

STRESSES IN THE SEAL AREA

Stresses in the vessel and chamber arise from two forms of loading, namely Lamé stresses [5], which result from the internal pressure, and residual stresses [6,7], which result from the autofrettage process.

The resultant hoop stress includes the Lamé hoop stresses

$$\sigma_{hoop-Lame}=\frac{a^2P_i}{c^2-a^2}\left(1+\frac{c^2}{r^2}\right) \tag{1}$$

and the autofrettage residual hoop stresses

$$\sigma_{hoop-autofrettage}=\sigma_{YS}\left[\left(\frac{a^2}{c^2-a^2}\right)\left(1+\frac{c^2}{r^2}\right)\left(\frac{\rho^2-c^2}{2c^2}-\ln\left(\frac{\rho}{a}\right)\right)+\left(\frac{\rho^2+c^2}{2c^2}-\ln\left(\frac{\rho}{r}\right)\right)\right] \tag{2}$$

which is valid in the range $a < r < \rho$, and

$$\sigma_{hoop-autofrettage}=\sigma_{YS}\left(1+\frac{c^2}{r^2}\right)\left[\frac{\rho^2}{2c^2}+\frac{a^2}{c^2-a^2}\left(\left(\frac{\rho^2-c^2}{2c^2}\right)-\ln\frac{\rho}{a}\right)\right] \tag{3}$$

which is valid in the range $\rho < r < c$. In these equations, a is the inside radius, c is the outside radius, r is the radial location of interest, P_i is the internal pressure, σ_{YS} is the material yield strength, and ρ defined as the elastic/plastic interface is

$$\rho=(c-a)*\frac{\%autofrettage}{100}+a \tag{4}$$

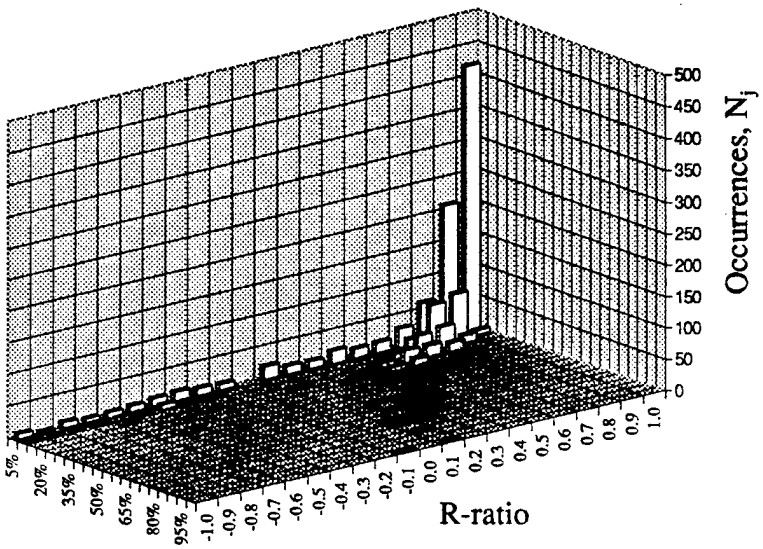

Figure 5. Histogram of occurrences, R-ratio, and hoop seal area strain range.

The superposition of these stresses results in the total hoop stress defined as

$$\sigma_{hoop-total}=\sigma_{hoop-autofrettage}+\sigma_{hoop-Lame} \tag{5}$$

The total hoop stress (at maximum pressure) from equation (5), and the resultant tensile hoop stress range for configuration #1 is plotted in Figure 3. The configuration #1 point lies directly on the hoop stress profile because there is no stress concentrator in the hoop orientation; thus equation (5) does not require a K_t scaling factor.

In a similar fashion, the Lamé radial stresses are expressed as

$$\sigma_{radial-Lame}=\frac{a^2P_i}{c^2-a^2}\left(1-\frac{c^2}{r^2}\right) \tag{6}$$

and the autofrettage residual radial stresses are

$$\sigma_{radial-autofrettage}=\sigma_{YS}\left[\left(\frac{a^2}{c^2-a^2}\right)\left(1-\frac{c^2}{r^2}\right)\left(\frac{\rho^2-c^2}{2c^2}-\ln\left(\frac{\rho}{a}\right)\right)+\left(\frac{\rho^2-c^2}{2c^2}-\ln\left(\frac{\rho}{r}\right)\right)\right] \tag{7}$$

which is valid in the range $a < r < \rho$, and

$$\sigma_{radial-autofrettage}=\sigma_{YS}\left(1-\frac{c^2}{r^2}\right)\left[\frac{\rho^2}{2c^2}+\frac{a^2}{c^2-a^2}\left(\left(\frac{\rho^2-c^2}{2c^2}\right)-\ln\frac{\rho}{a}\right)\right] \tag{8}$$

which is valid in the range $\rho < r < c$.

At first glance, it might seem that a typical stress concentration factor for configurations #2 and #3 in the R-L orientation would be greater than 3.0, because both configurations have a semicircular seal pocket whose depth is greater than its radius. However, this is not the case. Finite element modeling (FEM) of the seal and seal pocket areas was performed using Lamé and autofrettage loading, as well as a small preload on the seal, which prevents gases from escaping during the lower pressure stages of loading. The results of the FEM indicate that the K_t associated with the internal pressure Lamé loading is approximately 1.0. Since the seal pocket is pressurized to the same pressure as the vessel and chamber, it makes sense that the resultant stress concentration at the seal pocket notch would be negligible. For the autofrettage loading case, the FEM predicts stresses that are 60 percent higher than those predicted for the unnotched case. Hence, a K_t of 1.6 for the radial autofrettage stress was used. The resultant total radial stress can be represented as

$$\sigma_{radial-total}=1.6\ \sigma_{radial-autofrettatge}+\sigma_{radial-Lame} \tag{9}$$

Figure 3 shows the resultant radial stresses (at maximum pressure) for configurations #2 and #3—accounting for the previously described stress concentrators. In the next section, the maximum stress values (and stress ranges) from equations (5) and (9) are used to determine the local stress ranges at the failure locations.

LABORATORY MODELING OF SEAL AREA AND COMPARISON WITH FIELDED SYSTEM

Once the stresses typically seen in this type of pressure vessel were known, and the oscillatory behavior of the loadings had been well characterized, the next logical step was to determine how this combination affected the overall life of the component. The method of comparison uses the well-known Palmgren-Miner rule [8] as follows:

$$B_f \left[\Sigma \frac{N_j}{N_{fj}}\right]_{one\ repetition} = 1 \qquad (10)$$

In equation (10), N_j is the number of occurrences during the loading cycle at a particular strain level in the fielded system, N_{fj} is the experimentally-derived life the component should survive at the given strain level in the laboratory, and B_f is the total number of cumulative repetitions to failure.

Since N_j is already known (Figure 5), the only quantity left to establish is N_{fj}. A simple three-point bend specimen (Figure 6) with a semicircular notch that models the seal pocket was used. In this case, the notch detail is geometrically identical to the seal pocket notch in configurations #2 and #3, and possesses a K_t of 3.0 in uniaxial bend loading. Testing was conducted in load control for both A723 (Figure 7) and PH 13-8Mo (Figure 8) at three load ratios (R = 0.1, R = 0.25, and R = 0.5). Laboratory modeling was concentrated in the $1{,}000 < N_{fj} < 25{,}000$ cycles-to-failure region. The data were plotted and three distinct regions of fatigue were investigated. The data in the $1{,}000 < N_{fj} < 25{,}000$ region were curve fit with a log-log equation in the form of the Coffin-Manson equation. [8] The data in the $1 < N_{fj} < 25{,}000$ cycle region were then extrapolated to the true fracture strain for each material (at $N_{fj} \sim 1$ cycle) and curve fit with a similar log-log equation. The data in the $25{,}000 < N_{fj} <$ 1E+6 cycle region were extrapolated to the strain at a life of 1E+6 cycles and curve fit with a similar log-log equation. The latter two regions are expressed as dotted lines in Figures 7 and 8.

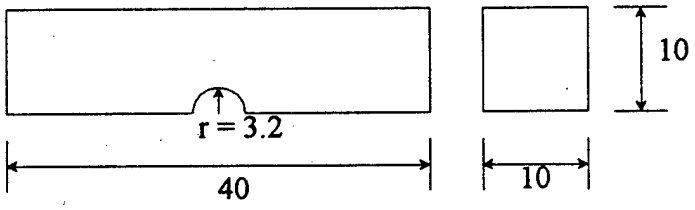

Figure 6. Specimen geometry modeling notch detail; all dimensions in millimeters.

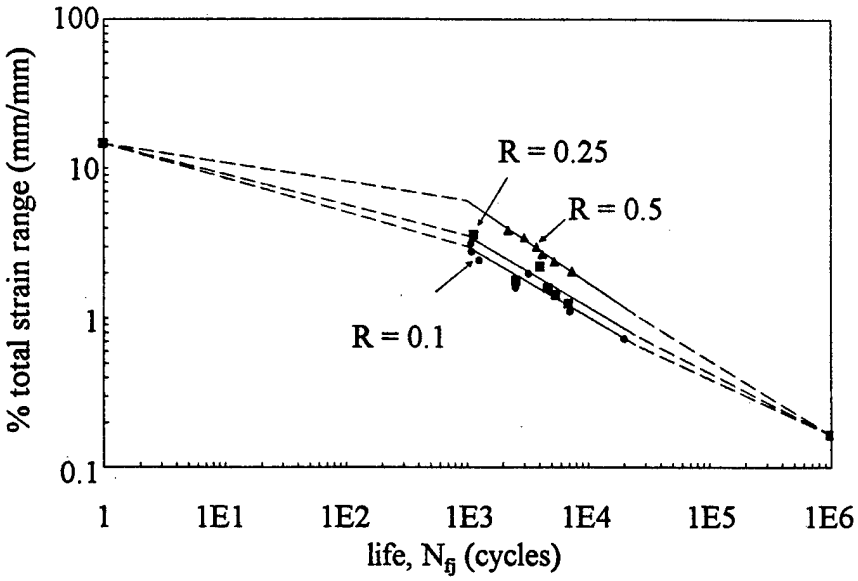

Figure 7. Low cycle fatigue data for A723 steel;
σ_{YS} = 1172 Mpa, K_t = 3.0.

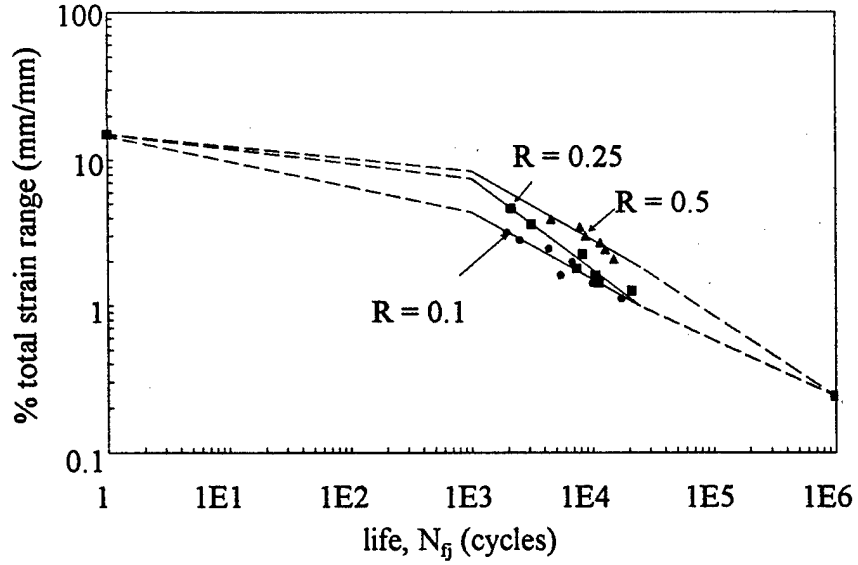

Figure 8. Low cycle fatigue data for PH 13-8Mo stainless steel;
σ_{YS} = 1276 Mpa, K_t = 3.0.

The effects of the compressive residual stresses for $R < 0$ have not been properly analyzed in the laboratory. Although no attempt was made to model these desirable residual stresses, it is known that their omission in the analysis would lead to conservative results. [9] In the analysis, all of the N_j with $R \leq 0.1$ were modeled in the laboratory at R = 0.1; those with $0.2 \leq R \leq 0.3$ were modeled in the laboratory at R = 0.25; and those with $R \geq 0.4$ were modeled at R = 0.5. The stresses predicted by equations (5) and (9) are in the elastic region. Therefore, Hooke's law ($\epsilon = \sigma/E$) was utilized to convert these seal pocket stresses into seal pocket strains. Once the conversion was made, the data in Figures 7 and 8 allowed N_{fj} to be calculated. At this point, B_f for each material and configuration could be determined.

Analysis of Configuration #1

Because configuration #1 failed in the C-R orientation, and the hoop stresses in the seal pocket region (equation (5)) were known to be tensile, the use of equation (10) predicted that the A723 steel vessel should survive a total of $B_f = 9{,}400$ repetitions before failure. The PH 13-8Mo chamber, which possesses better fatigue resistance than the A723 steel, should survive $B_f = 16{,}200$ repetitions before failure. Both predictions are orders of magnitude higher than the five cycles-to-failure in the fielded system.

Analysis of Configurations #2 and #3

Figure 2 shows that each of these configurations failed in the R-L orientation as a result of a radial tensile stress. However, according to the results in Figure 3, the radial stresses in the area of the seal pocket were compressive. The analysis used for configuration #1 predicted infinite life for these configurations, which we know was not the case.

Up to this point, the analysis has concentrated on Lamé and autofrettage stresses only. As is clearly seen from the previous analysis, these loadings alone could not have caused these failures; some other loadings that induce tensile stresses in the seal pocket region must be present.

OTHER SOURCES OF TENSILE LOADING

Because the source of radial tensile stresses could not be satisfactorily explained, other potential sources of loading were investigated. There is also compression loading consisting of two components (Figure 9a)—the compressive distributed loading of the seal on the seal pocket face ($\sigma_{\text{seal contact}}$), and the contact loading between adjacent sections ($\sigma_{\text{adjacent sections}}$) of the chamber and vessel. This type of loading has a direct analogy to the Timoshenko and Goodier [10] analysis of a hole in a plate under remote compression loading (Figure 9b). A hole in a plate under remote compressive loading will set up a tensile stress equal in magnitude to the remotely applied compressive stress (as shown in Figure 9b). Although the symmetry and loading are different in the two cases outlined in

Figures 9a and 9b, comparing the two situations is logical. The correct way to model the stresses resulting from these end loads is through finite element analysis. This work is currently underway.

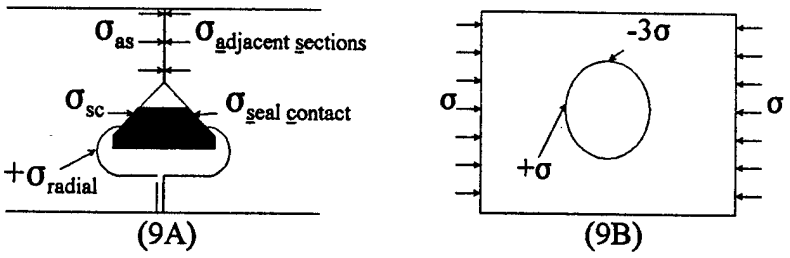

Figure 9. Comparison showing (a) possible source of tensile radial loads and (b) hole in a plate analogy.

Although the exact extent of the end loads is unknown, these stresses were analyzed using the shear strength of the thread that couples the chamber to the vessel and the seal contact stresses. The stress resulting from the adjacent sections was approximated by assuming that the threads that couple the adjacent sections were loaded to 25 percent of their maximum shear load [5], and that a 20 percent loss of loading was due to frictional effects. The seal contact stresses were approximated by assuming that a compressive stress equal in magnitude to the yield strength of the seal material was present. [11] Assuming these stresses and the previously mentioned Lamé and autofrettage stresses, the radial stress distribution of equation (9) can be modified to

$$\sigma_{radial\text{-}total}=1.6\ \sigma_{radial\text{-}autofrettatge}+\sigma_{radial\text{-}Lame}+\sigma_{adjacent\ sections}+\sigma_{seal\ load} \qquad (11)$$

The resultant stresses at the seal for configurations #2 and #3 were calculated, along with the critical flaw size (a_c) approximated by

$$K_{applied}=1.12\ \sigma_{applied}\sqrt{\pi\ a_c} \qquad (12)$$

The results can be seen in Table 2.

Table 2. Fracture Properties, Radial Stresses, and Calculated Critical Flaw Sizes

Material	Config.	K_{Ic}@ 25°C (MPa√m)	$\sigma_{radial\text{-}total}$ (MPa)	a_c (mm)	K_{IEAC}@ 25°C (MPa√m)	$\sigma_{radial\text{-}total\text{-}EAC}$ (MPa)	a_{EAC} (mm)
PH 13-8Mo	#2	148	670	12.4	15	950	0.063
	#3	148	766	9.5	15	961	0.062
A723	#2	123	670	8.5	15	950	0.063
	#3	123	766	6.5	15	961	0.062

Note that the critical flaw sizes calculated using the previously outlined approach estimate that the flaws necessary to initiate fast cracking range from 6.5 mm to 12.4 mm. It is extremely unlikely that a flaw of this magnitude existed. Flaws of this size would certainly have been detected in the inspection process.

ENVIRONMENTAL FRACTURE

Thus far, the investigation has shown that the oscillations could not have caused the earlier than anticipated failure of all three configurations; the investigation has identified the likely source of tensile loading in the seal region for configurations #2 and #3, and demonstrated that a classic fast fracture is unlikely because of the extremely large critical flaw sizes needed. This section takes the classic fracture mechanics approach one step further and investigates the possibility that environmentally-assisted cracking caused the premature failures.

Internal combustion gases present in the chamber and vessel are high in hydrogen concentration. In the presence of hydrogen, materials such as PH 13-8Mo and A723 are highly susceptible to accelerated cracking—to the point where fracture toughness values drop to dangerously low levels. Environmentally-assisted fracture toughness, K_{IEAC}, test results measured by Vigilante et al. [12] indicate that the threshold fracture toughness for both PH 13-8Mo and A723 is approximately 15 MPa√m—a small fraction of the K_{Ic} value in Table 2. Another critical feature needed for environmentally-assisted cracking is the presence of tensile stress. The previous section identified possible sources of tensile stresses. It is believed that hydrogen may be present at the fracture site long after the Lamé stresses have dissipated, accompanied by tensile radial stresses arising from the autofrettage, adjacent section contact, and seal load contact. Modifying equation (11) to reflect these changes results in

$$\sigma_{radial\text{-}total\text{-}EAC} = 1.6\ \sigma_{radial\text{-}autofrettatge} + \sigma_{adjacent\ sections} + \sigma_{seal\ load} \qquad (13)$$

The resulting stresses ($\sigma_{radial\text{-}total\text{-}EAC}$) and calculated critical flaw sizes (a_{EAC}) are shown in Table 2. The calculated critical flaw sizes in the presence of a hydrogen-rich environment are 0.062 mm to 0.063 mm. These small flaw sizes are much more likely to have been present than the larger a_c previously predicted.

SUMMARY

- The oscillations in the pressure vessel did not the cause the premature failures. They are an interesting oddity, but had no significant effect on the failure of the pressure vessel. The oscillations are of such a small magnitude that they are below the level of strain necessary to induce fatigue cracking.

- The driving force behind the C-R oriented failure in configuration #1 appears to be the autofrettage tensile hoop oriented stress. Moving the seal toward the inner radius and away from the tensile hoop stress region was justified. However, a deleterious tensile radial stress was encountered.

- The driving force behind the R-L oriented failures in configurations #2 and #3 is the tensile radial stress generated in the seal pocket notch. This stress is the result of the compressive end loading of the contacting chamber and vessel and the compressive seal loading. Eliminating this type of failure requires the removal of all compressive end loads. The end load associated with the adjacent sections contacting is easily corrected by ensuring that the chamber and vessel do not contact during the assembly process. There is no obvious method of removing the seal end loads with this design. Corrective actions are likely to result in a complete redesign of the seal and seal pocket. FEM of this area is necessary before a detailed recommendation can be made.

- Environmentally-assisted cracking caused by the hydrogen-rich by-products of the combustion process is the likely candidate for the premature failure of all three configurations. Calculation of the critical flaw sizes necessary to induce cracking in the presence of hydrogen is on the order of the size of flaws that could be present with this type of material and manufacturing process.

REFERENCES

1. API Specification 6A, "Specification for Wellhead and Christmas Tree Equipment," Seventeenth Edition, Section 10, February 1996.

2. Owens, J.H., "Seal Integrity and Connector Clamping Forces at the Subsea Wellhead," *15th Annual Offshore Technology Proceedings*, 1983.

3. *Aerospace Structural Metals Handbook*, Mechanical Properties Data Center, Belfour Stulen, Inc., 1971.

4. Troiano, E., Underwood, J.H., and Crayon, D., "Low Cycle Notched Fatigue Behavior and Life Predictions of A723 High Strength Steel," *Fatigue and Crack Growth: Environmental Effects, Modeling Studies and Design Considerations*, PVP-Vol 306, 1995.

5. Shigley, J.E., and Mitchell, L.D., *Mechanical Engineering Design*, Fourth Edition, McGraw Hill, New York 1983.

6. Prager, W., and Hodge, P.C., *Theory of Perfectly Plastic Solids*, J. Wiley and Sons, New York, 1951.

7. Hill, R., *The Mathematical Theory of Plasticity*, Oxford University Press, 1967.

8. Dowling, N.E., *Mechanical Behavior of Materials*, Prentice Hall, 1993.

9. Parker, A.P., "Stress Intensity Factors, Crack Profiles and Fatigue Crack Growth Rates in Residual Stress Fields," *Residual Stress Effects in Fatigue, ASTM STP 776*, American Society for Testing and Materials, Philadelphia, 1982.

10. Timoshenko, S.P., and Goodier, J.M., *Theory of Elasticity*, McGraw Hill, New York, 1970.

11. Roark, R.J., and Young, W.C., *Formulas for Stress and Strain*, McGraw Hill, New York, 1975.

12. Vigilante, G.N., Tauscher, S., Underwood, J.H., Crayon, D., Sage, T., and Troiano, E., "K_{IEAC} Test of High-Strength Steels and Nickel-Based Alloys in Hydrogen Environments Using the Bolt-Loaded Compact Specimen," *Fatigue and Fracture Mechanics, 28th Volume, ASTM STP 1321*, (J.H. Underwood, B.D. MacDonald, M.R. Mitchell, Eds.), American Society for Testing and Materials, Philadelphia, 1997.

TECHNICAL REPORT INTERNAL DISTRIBUTION LIST

	NO. OF COPIES
CHIEF, DEVELOPMENT ENGINEERING DIVISION	
ATTN: AMSTA-AR-CCB-DA	1
-DB	1
-DC	1
-DD	1
-DE	1
CHIEF, ENGINEERING DIVISION	
ATTN: AMSTA-AR-CCB-E	1
-EA	1
-EB	1
-EC	1
CHIEF, TECHNOLOGY DIVISION	
ATTN: AMSTA-AR-CCB-T	2
-TA	1
-TB	1
-TC	1
TECHNICAL LIBRARY	
ATTN: AMSTA-AR-CCB-O	5
TECHNICAL PUBLICATIONS & EDITING SECTION	
ATTN: AMSTA-AR-CCB-O	3
OPERATIONS DIRECTORATE	
ATTN: SIOWV-ODP-P	1
DIRECTOR, PROCUREMENT & CONTRACTING DIRECTORATE	
ATTN: SIOWV-PP	1
DIRECTOR, PRODUCT ASSURANCE & TEST DIRECTORATE	
ATTN: SIOWV-QA	1

NOTE: PLEASE NOTIFY DIRECTOR, BENÉT LABORATORIES, ATTN: AMSTA-AR-CCB-O OF ADDRESS CHANGES.

TECHNICAL REPORT EXTERNAL DISTRIBUTION LIST

	NO. OF COPIES
ASST SEC OF THE ARMY RESEARCH AND DEVELOPMENT ATTN: DEPT FOR SCI AND TECH THE PENTAGON WASHINGTON, D.C. 20310-0103	1
DEFENSE TECHNICAL INFO CENTER ATTN: DTIC-OCP (ACQUISITIONS) 8725 JOHN J. KINGMAN ROAD STE 0944 FT. BELVOIR, VA 22060-6218	2
COMMANDER U.S. ARMY ARDEC ATTN: AMSTA-AR-AEE, BLDG. 3022 AMSTA-AR-AES, BLDG. 321 AMSTA-AR-AET-O, BLDG. 183 AMSTA-AR-FSA, BLDG. 354 AMSTA-AR-FSM-E AMSTA-AR-FSS-D, BLDG. 94 AMSTA-AR-IMC, BLDG. 59 PICATINNY ARSENAL, NJ 07806-5000	 1 1 1 1 1 1 2
DIRECTOR U.S. ARMY RESEARCH LABORATORY ATTN: AMSRL-DD-T, BLDG. 305 ABERDEEN PROVING GROUND, MD 21005-5066	1
DIRECTOR U.S. ARMY RESEARCH LABORATORY ATTN: AMSRL-WT-PD (DR. B. BURNS) ABERDEEN PROVING GROUND, MD 21005-5066	1
COMMANDER ROCK ISLAND ARSENAL ATTN: SMCRI-SEM ROCK ISLAND, IL 61299-5001	1
COMMANDER U.S. ARMY TANK-AUTMV R&D COMMAND ATTN: AMSTA-DDL (TECH LIBRARY) WARREN, MI 48397-5000	1
COMMANDER U.S. MILITARY ACADEMY ATTN: DEPARTMENT OF MECHANICS WEST POINT, NY 10966-1792	1
U.S. ARMY MISSILE COMMAND REDSTONE SCIENTIFIC INFO CENTER ATTN: AMSMI-RD-CS-R/DOCUMENTS BLDG. 4484 REDSTONE ARSENAL, AL 35898-5241	2
COMMANDER U.S. ARMY FOREIGN SCI & TECH CENTER ATTN: DRXST-SD 220 7TH STREET, N.E. CHARLOTTESVILLE, VA 22901	1
COMMANDER U.S. ARMY LABCOM, ISA ATTN: SLCIS-IM-TL 2800 POWER MILL ROAD ADELPHI, MD 20783-1145	1

NOTE: PLEASE NOTIFY COMMANDER, ARMAMENT RESEARCH, DEVELOPMENT, AND ENGINEERING CENTER, BENÉT LABORATORIES, CCAC, U.S. ARMY TANK-AUTOMOTIVE AND ARMAMENTS COMMAND, AMSTA-AR-CCB-O, WATERVLIET, NY 12189-4050 OF ADDRESS CHANGES.

TECHNICAL REPORT EXTERNAL DISTRIBUTION LIST (CONT'D)

	NO. OF COPIES
COMMANDER U.S. ARMY RESEARCH OFFICE ATTN: CHIEF, IPO P.O. BOX 12211 RESEARCH TRIANGLE PARK, NC 27709-2211	1
DIRECTOR U.S. NAVAL RESEARCH LABORATORY ATTN: MATERIALS SCI & TECH DIV WASHINGTON, D.C. 20375	1
WRIGHT LABORATORY ARMAMENT DIRECTORATE ATTN: WL/MNM EGLIN AFB, FL 32542-6810	1
WRIGHT LABORATORY ARMAMENT DIRECTORATE ATTN: WL/MNMF EGLIN AFB, FL 32542-6810	1

NOTE: PLEASE NOTIFY COMMANDER, ARMAMENT RESEARCH, DEVELOPMENT, AND ENGINEERING CENTER, BENÉT LABORATORIES, CCAC, U.S. ARMY TANK-AUTOMOTIVE AND ARMAMENTS COMMAND, AMSTA-AR-CCB-O, WATERVLIET, NY 12189-4050 OF ADDRESS CHANGES.